# Effect of the addition of two pyrazole derivatives on behavior of the corrosion of mild steel in a 1 M HCl medium using experimental and theoretical insights

**H. Bouammali,[1] F. Abrigach,[1] S. Jerdioui,[1] B. El-Haitout,[2] A. Aouniti,[1] R. Touzani,[1] B. Hammouti[3,4]* and R. Salghi[2,3,4]**

*[1]Laboratory of Applied Chemistry and Environment (LCAE), Faculty of Sciences, University Mohammed First, Oujda, Morocco*
*[2]Laboratory of Applied Chemistry and Environment, ENSA, University Ibn Zohr, PO Box 1136, Agadir 80000, Morocco*
*[3]Euro-Mediterranean University of Fes, P.O. Box 15, 30070 Fez, Morocco*
*[4]Laboratory of Industrial Engineering, Energy and Environment (LI3E), SUP MTI, Rabat, Morocco*
**E-mail: hammoutib@gmail.com*

## Abstract

In this paper a comparative experimental and theoretical study of the inhibition capacity of two pyrazolic compounds, namely; Pyz1: *N*-(1*H*-pyrazol-1-yl)methyl)-5-bromopyridin-2-amine and Pyz2: ((1*H*-pyrazol-1-yl)methylamino) benzoic acid, against the corrosion of carbon steel was carried out in an acidic medium (1 M HCl at 30°C) according to different weight loss and electrochemical methods (potentiodynamic and electrochemical impedance spectroscopy, EIS). The analysis of the experimental results obtained revealed that Pyz1 is the most effective inhibitor, even at low concentrations and that its inhibition efficiency increased with the concentration of the inhibitor. The data obtained from the AC impedance measurements were analyzed to model the corrosion inhibition process using appropriate equivalent circuit models. The adsorption of these inhibitors on the carbon steel surface in acidic medium followed the Langmuir adsorption isotherm. The calculated $\Delta G^0_{ads}$ values indicate that these compounds are chemisorbed on the metal surface. Through a theoretical study, using the density functional theory (DFT) method, we demonstrated the existence of a correlation between molecular structure and their inhibitory power.

Received: February 4, 2024. Published: February 23, 2024 doi: 10.17675/2305-6894-2024-13-1-19

***Keywords:*** *pyrazole, C35E carbon steel, hydrochloric acid, corrosion, inhibition, adsorption, density functional theory method (DFT).*

## 1. Introduction

Corrosion is a major concern in industries that deal with metals, particularly mild steel. It can lead to significant economic losses and safety hazards in several industrial operations,

such as oil well acidizing and acid pickling. To mitigate corrosion, various methods have been explored, such as metal coating, surface treatment, cathodic or anodic protection, and the use of corrosion inhibitors. Among these methods, the use of corrosion inhibitors has gained significant attention, especially organic inhibitors, due to its effectiveness, eco-friendliness, and cost-effectiveness [1–6].

The inhibitory action of these organic compounds, which is generally independent of anodic and cathodic corrosion processes, is linked to the formation, by adsorption, of a more or less continuous barrier, but of finite thickness, which prevents access to the solution to the metal [7]. There are many organic compounds that can be used as inhibitors. From a "mother" molecule has a certain effectiveness, it is always possible to synthesize increasingly complex compounds with the aim of improving the inhibitory effectiveness. These organic compounds have at least one heteroatom serving as an active center for their fixation on the metal such as nitrogen (amines [8, 9], amides [10, 11], imidazolines [12, 13], triazoles [14, 15]), oxygen (acetylenic alcohols [16], carboxylates [17, 18], oxadiazoles [19, 20]), sulfur (derived from mercaptans [21–23], sulfoxides [24], thiazoles [25, 26]) or phosphorus (phosphonates [27–30]). One of the limitations in the use of these products can be the rise in temperature, as organic molecules are often unstable at high temperatures.

Pyrazolic compounds, part of the organic nitrogen compounds, are increasingly essential in the field of corrosion due to their strong physicochemical, biological and adsorption performances combined with good solubility in aggressive acidic environments, also low toxicity rate and low environmental risk [31]. Several studies have already been undertaken on the corrosion of steels [32, 33] as well as other metals and alloys [34, 35] in an aggressive acidic environment by organic compounds of the "pyrazole" type. Timoudan *et al.* [36] examined a novel pyrazol derivative for its ability to prevent corrosion of steel in acidic environments, the inhibition rate reached 97.2% at $10^{-3}$ M and 30°C. Another pyrazole product was synthesized by Verma *et al.* [30] using the microwave irradiation method, this product showed a better inhibition efficiency of 94.88% at 300 ppm in 1 M HCl. Adlani *et al.* [37] showed that the pyrazole-based organic compound, *N*-((3,5 dimethyl-1*H*-pyrazol-1-yl)methyl)-4-nitroaniline is a good anticorrosion inhibitor with maximum inhibition efficiency (*IE*%) of 95.1% at $10^{-3}$ M HCl. Boudjellal *et al.* [38] carried out their study on a pyrazolic carbothioamide compound and they showed that this compound has a high inhibition efficiency in 1 M HCl.

Also, Herrag *et al.* [39] showed that the inhibition efficiency of the organic compound 1-((benzyl-(2-cyano-ethyl)-amino)-methyl)-5-methyl-1*H*-pyrazole-3-carboxylic acid ethyl ester increases with its concentration to reach 98.5% at $10^{-3}$ M. Paul *et al.* [40] carried out another study on two carbohydrazide–pyrazole derivatives, they presented a notable attenuation capacity at 300 ppm in a HCl solution 15%.

Inspired by this work and given these very satisfactory results, we are strongly encouraged to look for new compounds of the same type to test their inhibitory effects on mild steel in a 1 M HCl acidic medium. For this, a comparative study of the inhibitory effect

of two pyrazoles, namely Pyz1: *N*-(1*H*-pyrazol-1-yl)methyl)-5-bromopyridin-2-amine and Pyz2: ((1*H*-pyrazol-1-yl) methylamino)benzoic acid on the corrosion of steel in 1 M HCl medium was carried out.

The choice of these compounds was based on their molecular structures, the Pyz1 and Pyz2 comprising functional groups and heteroatoms (nitrogen). To evaluate the inhibition properties of Pyz1 and Pyz2 on carbon steel corrosion in 1 M HCl, we used weight loss measurements, electrochemical impedance spectroscopy (EIS) techniques, potentiodynamic polarization, and the adsorption isotherm. Furthermore, the study of the correlation between the corrosion inhibitory activity of steel in 1 M HCl and the molecular structures of these two pyrazoles was carried out using the density functional theory method (DFT).

## 2. Experimental Section

### *2.1. Materials*

The mono-alkylated heterocyclic compounds Pyz1: *N*-(1*H*-pyrazol-1-yl)methyl)-5-bromopyridin-2-amine and Pyz2: acid ((1*H*-pyrazol-1-yl)methylamino) benzoic were prepared by mixing methylamines with one equivalent of (1H-pyrazol-1-yl) methanol under reflux for 4 hours in acetonitrile as solvent, according to the method described in the literature [41]. The chemical structures are presented in Table 1. The material used in the current paper was a carbon steel (Euronorm: C35E carbon steel and US specification: SAE 1035) with a chemical composition (in wt.%) of 0.370 C, 0.230 Si, 0.680 Mn, 0.016 S, 0.077 Cr, 0.011 Ti, 0.059 Ni, 0.009 Co, 0.160 Cu and the remainder iron (Fe). Before immersion in the medium, material specimens of C35E underwent a preparation process involving polishing by SiC paper having gradually finer particle sizes (from 120 to 1200); rinsed with distilled water, acetone and air drying, C35E samples were ready for further experiments. The acid solutions (1 M HCl) were prepared by dilution of an analytical reagent grade 37% HCl with double distilled water. The concentration range of Pyz1 and Pyz2 employed in this study was from $10^{-6}$ M to $10^{-3}$ M.

**Table 1.** Nomenclature and chemical structure of the investigated pyrazoles.

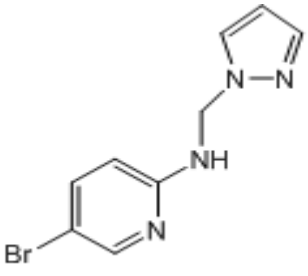


*N*-(1*H*-pyrazol-1-yl)methyl)-5-bromopyridin-2-amine

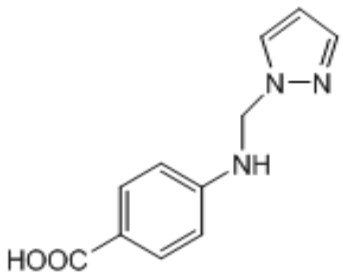


((1*H*-pyrazol-1-yl)methylamino) benzoic acid

### *2.2. Electrochemical apparatus and measurements*

In the open circuit potential method, the potential is fixed at the chosen value which corresponds to the time required to achieve equilibrium. Current intensity is measured between the working electrode and the platinum counter electrode. The electrochemical measurements are made with an assembly including a Tacussel PGZ 100 potentiostat controlled by "Voltalab" analysis software. The working electrode, in the form of a steel disc whose composition is given before, is introduced into a sample holder in polytetrafluoroethylene placed opposite the platinum counter electrode. 1 $cm^2$ of surface of the electrode is in contact with the mechanically stirred solution and deaerated by bubbling of nitrogen. All potentials are referenced to the saturated calomel electrode (SCE). The potential applied to the sample varies continuously, with a scanning speed equal to 1 mV/min, from −800 mV to −200 mV *vs.* SCE. The potential of the working electrode (WE) reaches its stability after waiting 30 minutes, the measurements can then be carried out. Electrochemical, impedance measurements are carried out using an electrochemical system (TACUSSEL PGZ 100) controlled by "Voltalab" analysis software. The results of this method are obtained in the form of diagrams, called Nyquist plots. The latter is processed using the Zview software by proposing an equivalent electrical circuit (CEE) respecting the essential conditions.

### *2.3. WL measurements*

The gravimetric measurements were carried out at the definite time interval of 24 h at room temperature 30°C using an analytical balance (precision 0.1 mg). The steel specimens used had a rectangular form (length = 5 cm, width = 2 cm, thickness = 0.3 cm). Gravimetric experiments were carried out in a double glass cell equipped with a thermostated cooling condenser containing 250 ml of non-de-aerated test solution. After immersion period, the steel specimens were withdrawn, carefully rinsed with bidistilled water, ultrasonically cleaned in acetone, dried at room temperature and then weighed. Triplicate experiments were performed in each case and the average value of the weight loss was used to calculate the corrosion rate ($C_R$) in mg/$cm^2$·h and the inhibition efficiency $\eta_{WL}$ in percent (%). These were calculated from Equations 1 and 2 [42], respectively:

$$C_R = \frac{W_b - W_a}{AT} \tag{1}$$

$$\eta_{WL}(\%) = \left(1 - \frac{W_i}{W_0}\right) \cdot 100\% \tag{2}$$

In this context, $W_b$ and $W_a$ represent the weight of the specimen before and after immersion in the tested solution, $W_0$ and $W_i$ denote the corrosion weight losses of carbon steel in uninhibited and inhibited solutions, respectively. "A" stands for the total area of the steel

specimen (measured in square centimeters), and *t* indicates the exposure time (measured in hours).

### *2.4. Theoretical study by DFT*

The study of the correlation between the inhibitory activity of steel corrosion in 1 M HCl and the molecular structure of pyrazoles is conducted using the Density Functional Theory (DFT) method at the B3LYP level with the 6-31G (d, p) basis set. Quantum chemical indices, namely, the dipole moment (μ), total energy (TE), Highest Occupied Molecular Orbital (HOMO) and Lowest Unoccupied Molecular Orbital (LUMO) energies, the energy gap ($\Delta E$), and softness (σ), are determined.

#### *MD simulation*

The adsorption of the pyrazole derivatives on the mild steel surface in 1 M HCl solution was also investigated using molecular dynamics simulations. In this method, we used the Material Studio software 6.0, to simulate the interaction between the corrosion inhibitors and the steel surface. The simulation was carried out with the Forcite Module in Materials Studio, which is based on classical force field parameters. The iron surface was cleaved into the (110) plane and extended to a (5×5) supercell. The simulation box was constructed with three layers of iron atoms and surrounded by a water box to simulate the HCl solution environment. The solution box containing 500 $H_2O$ molecules, 10 $H_3O^+$ ions, 10 $Cl^-$ ions, and the inhibitor molecules (Pyz1 or Pyz2), all collected by the Amorphous cell module. The simulation then used the COMPASS force field to calculate the intermolecular and atomic forces, and was run with applying a simulation time of 5000 picoseconds, a time step of 1 femtosecond, and a temperature of 298 Kelvin, and calculations carried out at a "Fine" quality.

#### *First-principles (ab initio) DFT simulations*

In addition of to the molecular dynamics simulation, and the DFT calculations, we also employed First-principles (*ab initio*) DFT method to further investigate the interaction between the pyrazole derivatives and the mild steel surface. The *ab initio* method is a semi-empirical quantum mechanical method that combines elements of density functional theory and molecular mechanics. In this work, we used the trans 3d parameters of Slater Koster set to simulate the electronic structure and energetics of the corrosion inhibitors adsorbed on the steel surface. Besides, The SCC (self-consistent charge) scheme was used to include polarization effects in the system, allowing for a more accurate representation of the intermolecular interactions. A "Fine" quality was applied to the CASTEP module to ensure accurate and reliable results, with setting the k-points to 8×8×8 grid for Brillouin zone sampling. The iron surface was again cleaved into the plane and extended to a (5×5) supercell, similar to the molecular dynamic simulations. On the other hand, the partial density of states analysis was conducted by placing the pyrazole derivatives at two different positions above the steel surface (near the surface and 7 Å above), and calculating the

electronic structure properties to gain insight into the adsorption mechanism and the stability of the inhibitor-steel complex. Prior running the first-principles (*ab initio*) DFT calculations, the inhibitor positioned with a planar geometry above the Fe (110) surface, and the two lower layers of the supercell were fixed to mimic the bulk steel. To calculate the interaction energy of the adsorption system the formula below was followed:

$$E_{ads} = E_{mol/surface} - (E_{surf} + E_{mol})$$

## 3. Results and Discussion

### *3.1. Evaluation gravimetric tests*

The study of the inhibitory action of the two compounds Pyz1 and Pyz2 on the corrosion of steel by gravimetry was carried out in the 1 M HCl, in absence and in the presence of organic compound for a period of 4 hours at 35°C (Figure 1). The inhibitory efficiency $\eta_{WL}$ (%) was evaluated by measuring the corrosion rate ($C_R$). The results of the comparative study shown in Table 2 show that the addition of these two pyrazole compounds tested is accompanied by a reduction in the corrosion rate. Indeed, the variation in $\eta_{WL}$(%) with concentration of pyrazolic product, presented in Figure 2, showed that the protection inhibition efficiency increased with the increase of the Pyz concentration. The inhibitory effect is pronounced in the case of pyrazole Pyz1 with 98% and therefore, it turns out to be the best inhibitor compared to Pyz2 at the maximum concentration of $10^{-3}$ M after 24 h of immersion in 1 M HCl.

**Table 2.** Corrosion parameters obtained from weight loss measurements for carbon steel in 1 M HCl containing various concentrations of "Pyz1 and Pyz2" at 30°C.

| **Inhibitor** | **Concentration, M** | **$C_R$, mg/cm$^2$·h** | **$\eta_{WL}$, %** |
|---|---|---|---|
| Blank | 1 M | 0.75 | – |
| Pyz1 | $10^{-6}$ | 0.44 | 41 |
| | $5\cdot10^{-6}$ | 0.38 | 49 |
| | $10^{-5}$ | 0.28 | 63 |
| | $5\cdot10^{-5}$ | 0.21 | 72 |
| | $10^{-4}$ | 0.14 | 81 |
| | $5\cdot10^{-4}$ | 0.06 | 92.4 |
| | $10^{-3}$ | 0.016 | 98 |
| Pyz2 | $10^{-6}$ | 0.32 | 57 |
| | $5\cdot10^{-6}$ | 0.31 | 59 |
| | $10^{-5}$ | 0.27 | 64 |
| | $5\cdot10^{-5}$ | 0.24 | 68 |

| Inhibitor | Concentration, M | $C_R$, mg/cm$^2$·h | $\eta_{WL}$, % |
|---|---|---|---|
| | $10^{-4}$ | 0.14 | 81 |
| | $5 \cdot 10^{-4}$ | 0.099 | 87 |
| | $10^{-3}$ | 0.059 | 92 |

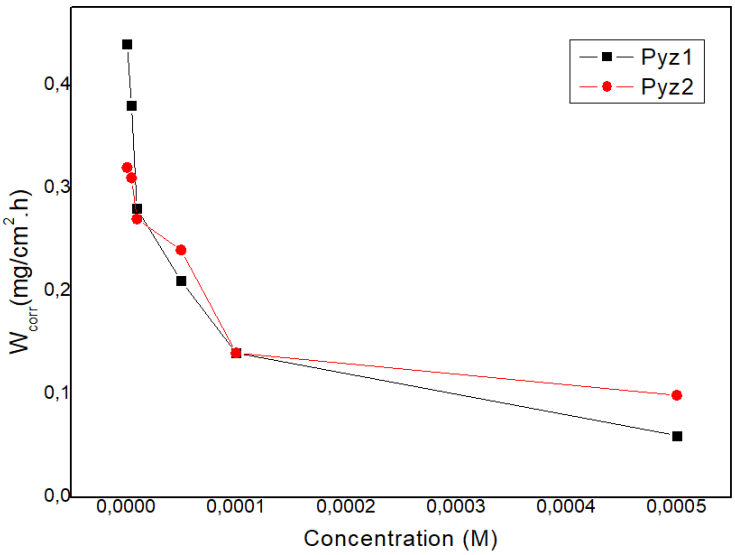


**Figure 1.** Evolution of the corrosion rate as a function of the concentration of Pyz1 and Pyz2.

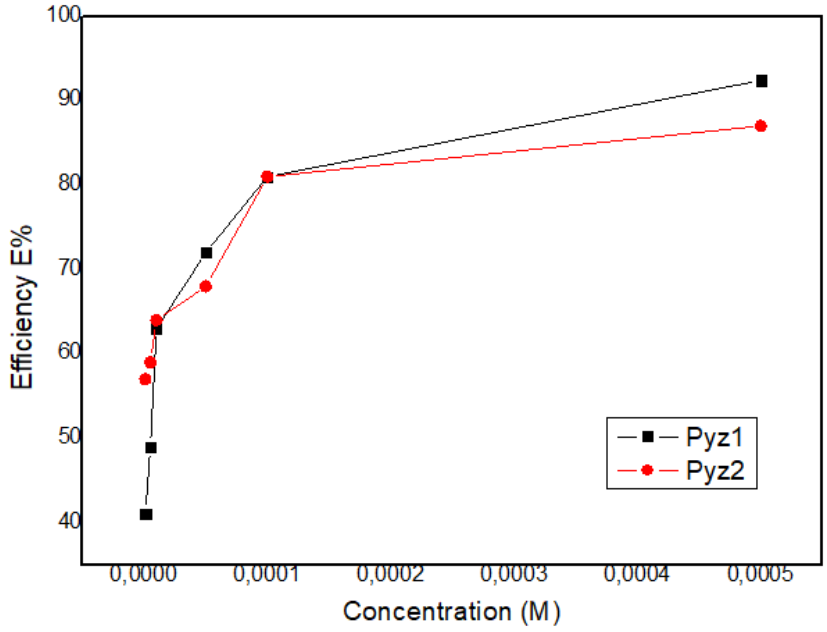


**Figure 2.** Evolution of inhibitory efficiency as a function of the concentration of Pyz1 and Pyz2.

### *3.2. Electrochemical study*

The electrochemical method used to characterize the metal/electrolyte interface is based on the plotting of polarization curves in a logarithmic scale, which allows us to directly access the value of the current by a simple reading on the graph.

#### *3.2.1. Stationary methods (polarization curves)*

The polarization curves in the absence and presence of Pyz1 and Pyz2, at different concentrations, in 1 M HCl medium at 35°C are shown in (Figure 3) and (Figure 4). In view of the results obtained, we can note that the addition of pyrazole compounds systematically results in a reduction in the cathodic and anodic current densities. The evolution of the $\log i = f(E)$ curves as a function of the concentration of Pyz1 and Pyz2 is approximately identical. The values of corrosion current density ($i_{corr}$), the corrosion potential ($E_{corr}$), the cathodic and anodic Tafel slopes ($\beta_c$ and $\beta_a$) and the inhibitory efficiency *IE*% for different concentrations of Pyz1 and Pyz2 in HCl medium are reported in Table 3.

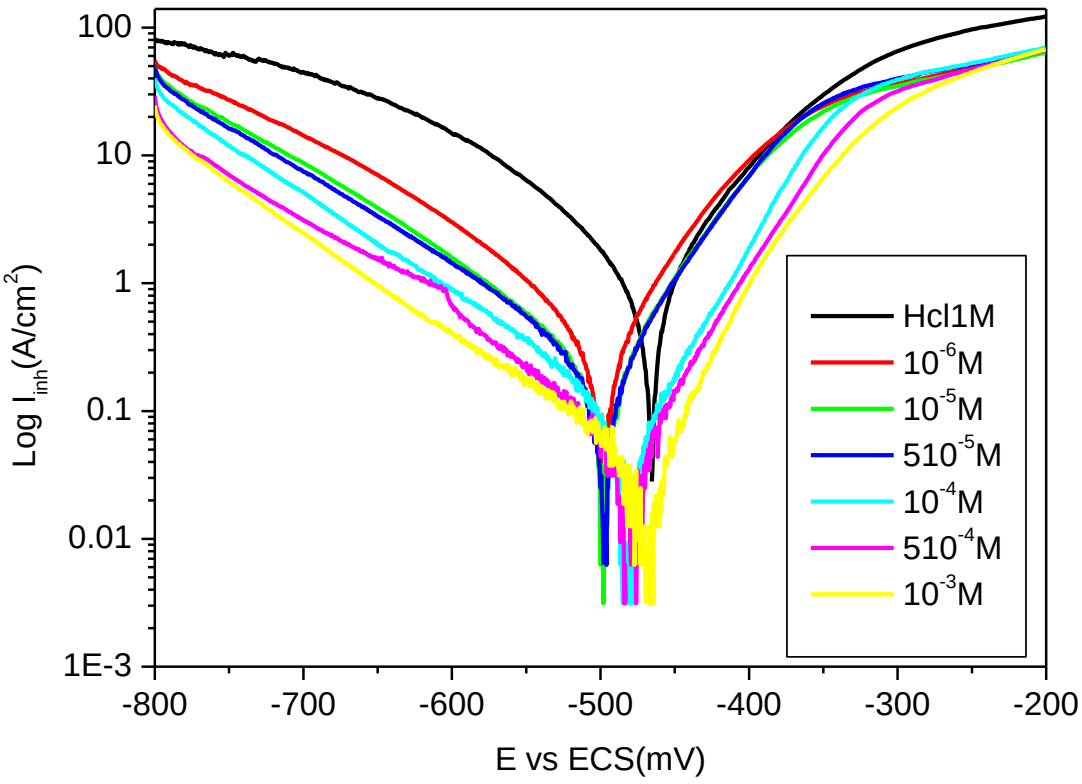


**Figure 3.** Polarization curves of steel in 1 M HCl without and with addition of different concentrations of Pyz1.

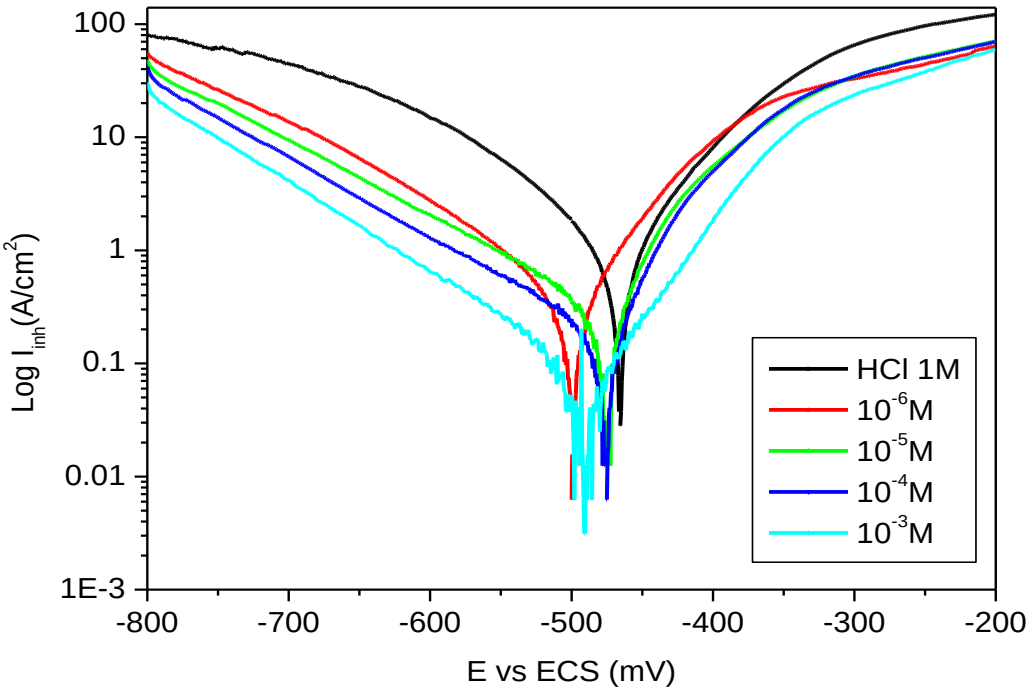


**Figure 4.** Polarization curves of steel in 1 M HCl without and with addition of different concentrations of Pyz2.

**Table 3.** Electrochemical parameters for different concentrations of Pyz1 and Pyz2.

| **Inhibitors** | **Concentration, M** | $E_{corr}$ ***vs.*** **(SCE), mV** | $i_{corr}$, **μA/cm²** | ***IE*%** |
|---|---|---|---|---|
| Blank | 1 | –466 | 530 | – |
| Pyz1 | $10^{-6}$ | –499 | 223 | 58 |
| | $10^{-5}$ | –498 | 217 | 59 |
| | $5 \cdot 10^{-5}$ | –498 | 130 | 75 |
| | $10^{-4}$ | –484 | 93 | 82 |
| | $5 \cdot 10^{-4}$ | –481 | 48 | 91 |
| | $10^{-3}$ | –472 | 22 | 96 |
| Pyz2 | $10^{-6}$ | –500 | 255 | 52 |
| | $10^{-5}$ | –476 | 193 | 63 |
| | $10^{-4}$ | –476 | 101 | 81 |
| | $10^{-3}$ | –496 | 56 | 89 |

The analysis of Table 3 and polarization curves previously obtained allowed us to note for the two species that: 1) in the cathodic domain, the addition of inhibitor reduces current densities. The slight modification of the cathodic Tafel slopes, in the absence and presence

of the inhibitor, show that the proton reduction reaction on the surface of the steel is not modified by the addition of the inhibitor and that it is done according to a pure activation mechanism; 2) in the same way, in the anodic domain, the addition of the inhibitor results in a reduction in the anodic current densities. In addition, we note for all the concentrations studied, the presence of two linear portions in the case of a strong anodic overvoltage (potential applied to the sample of up to –200 mV/SCE).

When a desorption potential $E_d$ [43], also called potential of non-polarizability by Heusler and Cartledge [44] or by Bartos and Hackerman [45], is exceeded, the inhibitor practically no longer has effect on the anodic curves; the anodic current density then increases rapidly and the steel is dissolved in the region of high overvoltages. This behavior has been widely documented in the case of steel in hydrochloric acid solutions [46]. The rapid growth of the anodic current, after the potential $E_d$, is attributed to the desorption of the inhibitor molecules adsorbed on the surface of the metal. However, even though the inhibitor resorbs from the metal surface, it inhibits corrosion since anodic current densities remain slightly lower than those of blank. Which clearly indicates that the adsorption and desorption of pyrazoles depends on the electrode potential. In general, we can see that as a function of the concentration the values of $E_{corr}$ are moving slightly towards more positive values, and that gradually that the inhibitor concentration increases, the corrosion current densities ($i_{corr}$) decrease sharply.

In addition, the two partial anodic and cathodic currents are also reduced. These observations confirm the mixed character and clearly show that the inhibitor reduces the speed of anodic dissolution of steel and that of the reduction of the $H^+$ proton.

### *3.2.2. Electrochemical impedance spectroscopy*

Measuring electrochemical impedance consists of studying the response of an electrochemical system following a disturbance which is, most often, an alternating signal of low amplitude. The advantage of this technique is to differentiate reaction phenomena by their relaxation time. Only fast processes are characterized at high frequencies; when the applied frequency decreases, the contribution of slower steps will appear, such as transport or diffusion phenomena in solution [46]. The impedance spectra obtained at the corrosion potential are recorded after 30 minutes of immersion in 1 M HCl medium at 35°C for different concentrations of Pyz1 and Pyz2 (for the stabilization of the corrosion potential). The Nyquist and Bode diagrams obtained for Pyz1 and Pyz2 are presented respectively in (Figure 5) and (Figure 6).

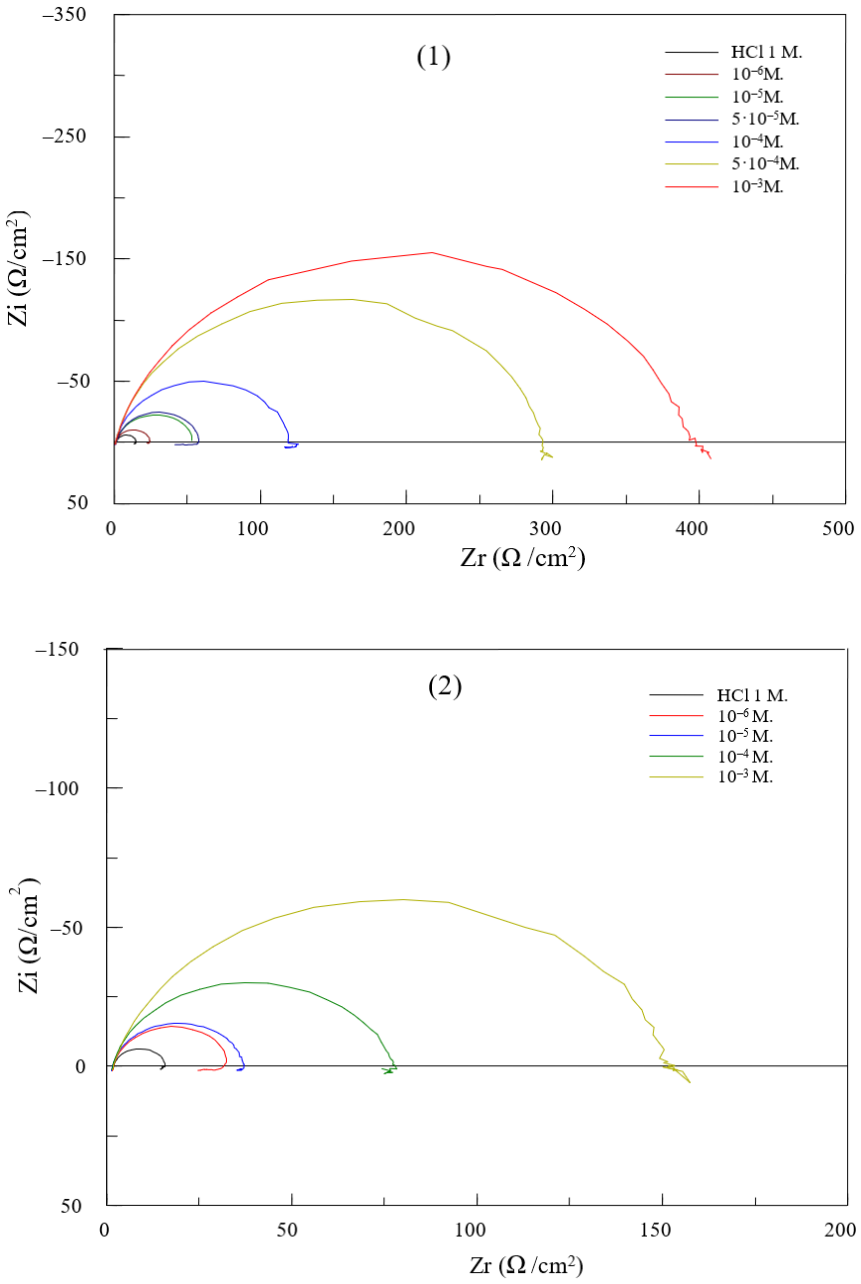


**Figure 5.** Nyquist diagrams of the steel in 1 M HCl containing different concentrations of Pyz1 (1) and Pyz2 (2) at 35°C.

These diagrams are represented by more or less flattened capacitive loops, presenting a phase shift with respect to the real axis (Figures 5 and 6). This type of diagram is generally interpreted as a charge transfer mechanism on an inhomogeneous surface [47]. In fact, only one time constant is detected on the Bode diagram (Figure 7, 8 and 9), the same behavior is observed on the other compound. The sizes of the capacitive loops increase with increasing inhibitor concentration. The representative equivalent electric circuit (EEC) in the case of the adsorption of Pyz1 and Pyz2 is shown in Figure 10. This circuit consists of a constant

phase element (CPE), used to account for inhomogeneities, the electrolyte resistance $R_s$, and the charge transfer resistance ($R_{ct}$) which is in series with the inductive elements ($L$) and $R_3$ which are in parallel (for concentrations of $10^{-6}$ M, $10^{-5}$ M of Pyz2).

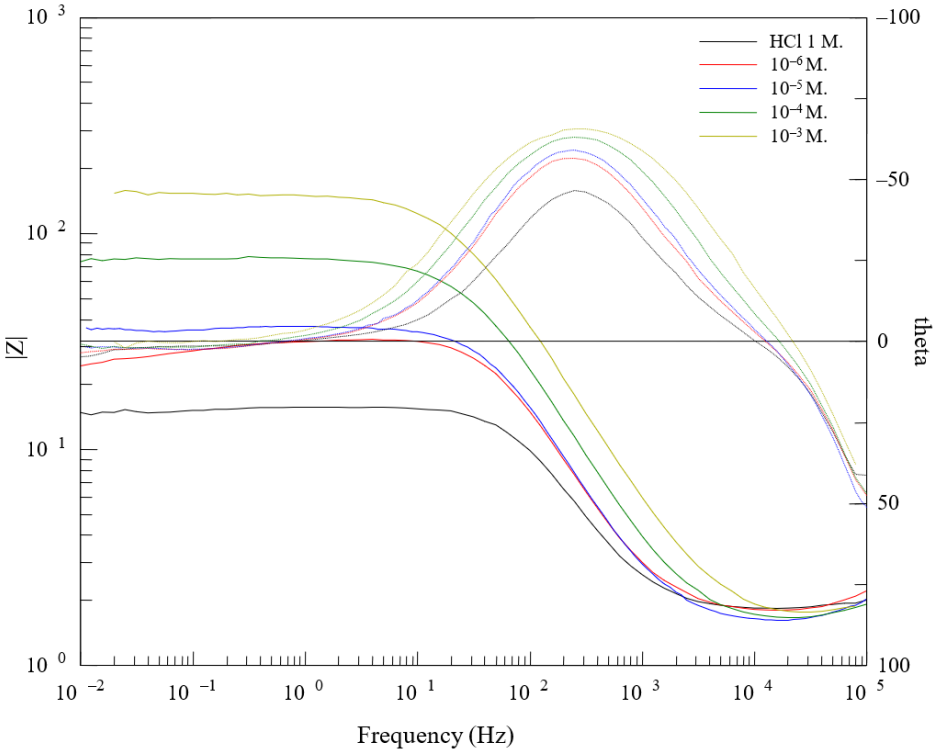


**Figure 6.** Bode diagrams of the steel in 1 M HCl containing different concentrations of Pyz2 at 35°C.

These diagrams are represented by more or less flattened capacitive loops, presenting a phase shift with respect to the real axis (Figures 5 and 6). This type of diagram is generally interpreted as a charge transfer mechanism on an inhomogeneous surface [47]. In fact, only one time constant is detected on the Bode diagram (Figure 7, 8 and 9), the same behavior is observed on the other compound. The sizes of the capacitive loops increase with increasing inhibitor concentration. The representative equivalent electric circuit (EEC) in the case of the adsorption of Pyz1 and Pyz2 is shown in Figure 10. This circuit consists of a constant phase element (CPE), used to account for inhomogeneities, the electrolyte resistance $R_s$, and the charge transfer resistance ($R_{ct}$) which is in series with the inductive elements ($L$) and $R_3$ which are in parallel (for concentrations of $10^{-6}$ M, $10^{-5}$ M of Pyz2).

An excellent parametric fit of the experimental impedance spectra for these two pyrazole compounds was obtained using the new model (a, b). The experimental and simulated spectra are well correlated. The values of different parameters from the parametric adjustment using CPE are listed in (Tables 4 and 5).

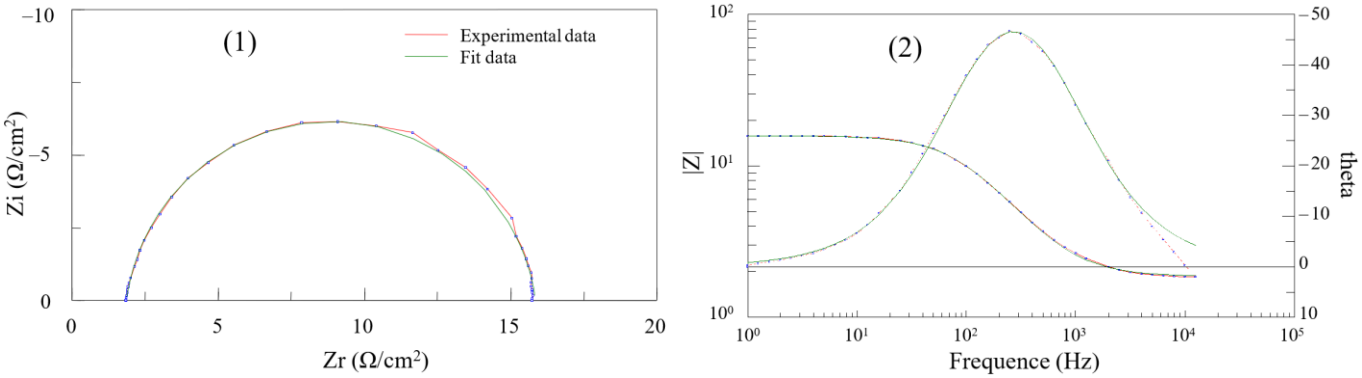


**Figure 7.** Nyquist (1) and Bode (2) representations of the steel surface in a 1 M HCl solution, experimental curve, fitted curve.

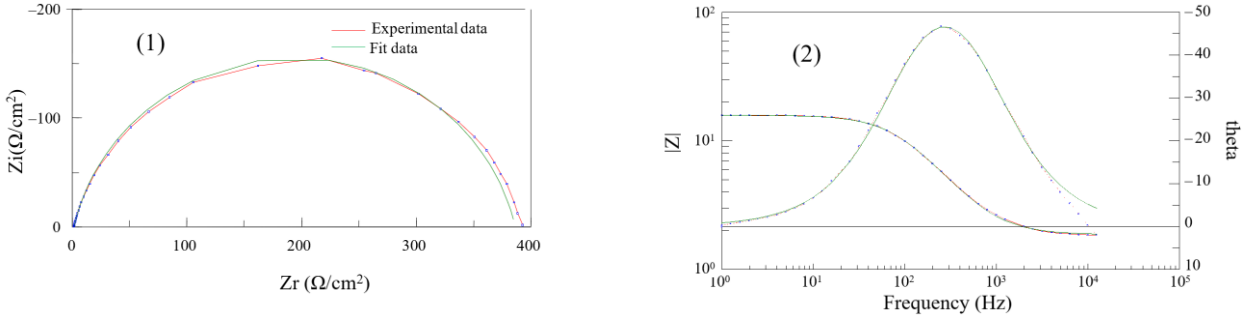


**Figure 8.** Nyquist (1) and Bode (2) representations of the steel interface in a 1 M+$10^{-3}$ M HCl solution of Pyz1 with: experimental curve, fitted curve.

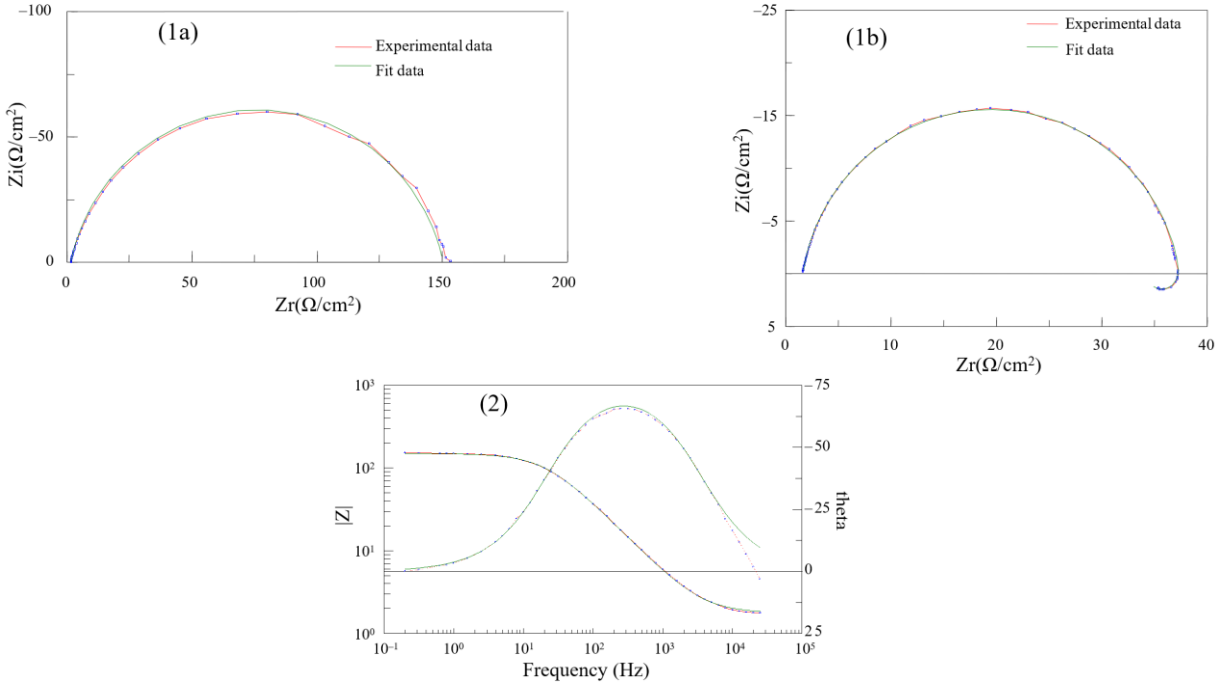


**Figure 9.** Nyquist (1) and Bode (2) representation of the steel interface in a HCl 1 M+$10^{-3}$ M (1a) and $10^{-5}$ M (1b) of Pyz2 solution with: experimental curve, fitted curve.


**Figure 10.** Model of the equivalent circuit for the steel/1 M HCl interface: (a) in the presence of Pyz1 and (b) in the presence of Pyz2 at $10^{-5}$ M.

**Table 4.** Electrochemical parameters and corrosion inhibitory efficiency of steel in 1 M HCl without and with addition of different concentrations of Pyz1 at 35°C.

| Conc., M | $R_s$, Ω·cm$^2$ | $R_{ct}$, Ω·cm$^2$ | $10^4 \cdot A_d$, W$^{-1}$·s$^n$·cm$^{-2}$ | $n_d$ | $C_{dl}$, µF·cm$^{-2}$ | *IE*, % |
|---|---|---|---|---|---|---|
| Blank | 1.863 | 14 | 2,31 | 0,91 | 132 | |
| $1 \cdot 10^{-6}$ | 1.8 | 23.6 | 1.91 | 0.912 | 114 | 41 |
| $1 \cdot 10^{-5}$ | 1.79 | 52.5 | 1.36 | 0.905 | 82 | 73 |
| $5 \cdot 10^{-5}$ | 1.86 | 57 | 1.48 | 0.896 | 82 | 76 |
| $1 \cdot 10^{-4}$ | 1.65 | 119 | 1.10 | 0.892 | 65 | 88 |
| $5 \cdot 10^{-4}$ | 1.72 | 290 | 0.79 | 0.879 | 46 | 95 |
| $1 \cdot 10^{-3}$ | 1.65 | 385 | 0.89 | 0.865 | 52 | 96 |

**Table 5.** Electrochemical parameters and corrosion inhibitory efficiency of steel in 1 M HCl without and with addition of different concentrations of Pyz2 at 35°C.

| Conc., M | $R_s$, Ω·cm$^2$ | $R_{ct}$, Ω·cm$^2$ | $10^4 A_d$, W$^{-1}$·s$^n$·cm$^{-2}$ | $n_d$ | *L* | *R* | $C_{dl}$, µF·cm$^{-2}$ | *IE*, % |
|---|---|---|---|---|---|---|---|---|
| Blank | 1.863 | 14 | 2.31 | 0.91 | – | – | 132 | |
| $1 \cdot 10^{-6}$ | 1.97 | 24 | 1.87 | 0.909 | 1.8 | 2.86 | 112 | 48 |
| $1 \cdot 10^{-5}$ | 1.65 | 33 | 1.63 | 0.91 | 5.05 | 3.13 | 99 | 60 |
| $1 \cdot 10^{-4}$ | 1.66 | 75 | 1.32 | 0.884 | – | – | 72 | 82 |
| $1 \cdot 10^{-3}$ | 1.75 | 150 | 0.956 | 0.867 | – | – | 50 | 91 |

By analyzing the results, we can make the following remarks: 1) The values of the transfer resistance ($R_t$) become greater with the increase in the concentration of Pyz1 and Pyz2. The inhibitory efficiency of these two inhibitors, calculated from these parameters, evolves in the same way as the charge transfer resistance ($R_t$) and reaches a value of 96% in the case of Pyz1. 2) With the addition of Pyz1 and Pyz2, the capacity of the double layer ($C_{dl}$) decreases and goes from 114 µF·cm$^2$ to 52 µF·cm$^2$ in the presence of Pyz1 at $10^{-3}$ M and the 112 µF·cm$^2$ at 50 µF·cm$^2$ in the presence of Pyz2 at $10^{-3}$ M. This reduction is

associated with the adsorption of organic molecules on the surface of the steel [56]. Indeed, the more the inhibitor adsorbs, the more the thickness of the organic deposit increases and the more the capacity of the double layer decreases according to the expression presented in the Helmotz model:

$$C_{\mathrm{dl}} = \frac{\varepsilon_0 \varepsilon}{e} S \tag{3}$$

where $e$ is the thickness of the deposit, $S$ is the surface of the electrode, $\varepsilon_0$ is the permittivity of the medium and $\varepsilon$ is the dielectric constant.

– The values of $A$ decrease when the concentration of pyrazoles increases and the values of $A$ are lower than those measured in the absence of inhibitor. This result suggests that this reduction is due to a reduction in contact surface linked to the adsorption of the inhibitor.

– At low frequencies, the appearance of an inductive loop for concentrations of $10^{-5}$ M and $10^{-6}$ M of Pyz2 can be attributed to the relaxation of the species adsorbed on the surface of the electrode such as $Cl^{-}_{ads}$ and $H^{+}_{ads}$.

### *3.3. Thermodynamic study*

During acid pickling, carried out at high temperatures, the role of inhibitors is to protect metal installations against acid attacks [47]. During mechanical machining (cutting, drilling, *etc.*), local heating, largely due to the frictions of the surfaces at the level of the machined parts or cutting tools, is also constated. These temperature rises can have a significant impact on the formation of the inhibitor layer and its stability. Temperature constitutes, in fact, one of the factors that can simultaneously modify the behavior of inhibitors and that of substrates in a given aggressive environment. The increase in temperature would thus promote the desorption of the inhibitor and lead to rapid dissolution of the organic compounds or complexes formed, thus causing a weakening of the corrosion resistance of the steel [48].

The influence of temperature on the effectiveness of inhibitors in an acidic environment has been the subject of numerous publications, Aljourani *et al.* studied the effect of temperature on the effectiveness of benzimidazole and these derivatives with respect to the corrosion of steel in an acidic 1 M HCl medium in the range 25–55°C [49]. This study revealed a decrease in the protective power of the inhibitor with an increase in temperature. Tebbji *et al.* [50] came to the same findings during their tests on the inhibitory action of organic compounds of the bipyrazole type and pyridazine derivatives on the corrosion of iron in an acidic environment in the temperature range 20–80°C.

However, despite the large number of studies that have observed a decrease in inhibitory efficiency with temperature [51], other studies have highlighted the opposite trend [52]. Bayol *et al.* [53] thus showed an increase, with temperature, in the inhibitory effectiveness of hexamethylenetetramine with respect to the corrosion of steel in 0.3 M HCl in the 20–50°C interval. In order to determine the effect of this variable on the inhibitory power of pyrazole compounds on mild steel, we carried out a gravimetric characterization at

different temperatures (35°C, 45°C, 55°C, 65°C and 80°C), for two hours of immersion in order to determine the corrosion rate of mild steel in 1 M HCl without and with addition of $10^{-3}$ M Pyz1 and Pyz2. The values of the corrosion rates and the corresponding inhibitory efficiencies as a function of temperature are collected in Table 6.

**Table 6.** Influence of temperature on the corrosion parameters of steel in 1 M HCl+$10^{-3}$M medium of Pyz1 and Pyz2.

| Compound | Temperature, °C | $W_{corr}$, mg/cm$^2$·h | *IE*% |
|---|---|---|---|
| HCl (1 M) | 35 | 0.47 | – |
| | 45 | 1.23 | – |
| | 55 | 2.96 | – |
| | 65 | 6.68 | – |
| | 80 | 22.96 | – |
| Pyz1 | 35 | 0.056 | 88 |
| | 45 | 0.14 | 87 |
| | 55 | 0.28 | 90 |
| | 65 | 0.51 | 92 |
| | 80 | 1.89 | 92 |
| Pyz2 | 35 | 0.036 | 92 |
| | 45 | 0.082 | 87 |
| | 55 | 0.124 | 96 |
| | 65 | 0.21 | 97 |
| | 80 | 0.58 | 97 |

The results in this table show that the corrosion rate in HCl (1 M) increases with increasing temperature. In the case of iron corrosion in an acidic environment, many authors use the Arrhenius equation (4) to account for the effect of temperature on the corrosion rate.

$$\ln(w) = \frac{E_a}{RT} + \ln(A) \quad (4)$$

In this relation, $E_a$ represents the apparent activation energy and $A$ the Arrhenius pre-exponential parameter. Figure 11 represents the plot in Arrhenius coordinates of the average corrosion rate of steel in HCl (1 M) in absence and in presence of the pyrazoles tested at $10^{-3}$ M. The activation parameters obtained and calculated from these lines are given in Table 7.

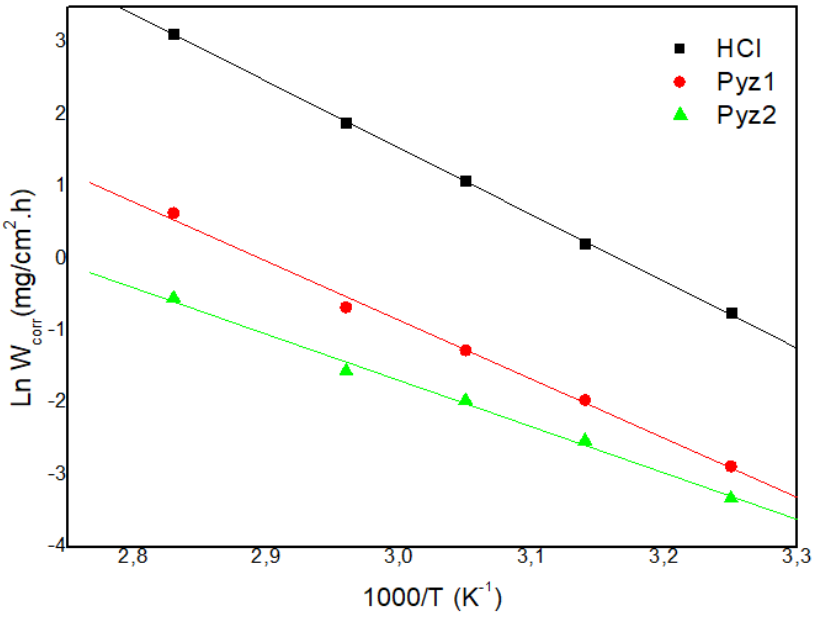


**Figure 11.** Arrhenius lines of steel in HCl (1 M) medium without and with addition of the different pyrazolic compounds Pyz1 and Pyz2 at $10^{-3}$ M.

**Table 7.** Steel activation parameters in HCl medium (1 M) without and with addition of different pyrazoles.

| **Compounds** | **HCl (1 M)** | **Pyz1** | **Pyz2** |
|---|---|---|---|
| $E_a$, kJ/mol | 77 | 68 | 55 |

The variations of $\ln(W_{corr})$ as a function of the reciprocal of the absolute temperature are in the form of straight lines (Figure 11). The inhibitors studied adsorb on the surface by covalent bonds (chemisorbed to the surface of the electrode). Indeed, the $E_a$ values for our pyrazolic compounds at different concentrations are higher than the $E_a$ value obtained for the solution without inhibitor.

### *3.4. Adsorption isotherm*

The inhibition of metal corrosion by organic compounds is explained by their adsorption on the metal surface. Adsorption isotherms are then an important complement capable of determining the mechanism which leads to the adsorption of these organic compounds on the surface. In order to obtain the isotherm, the coverage rate of the metal surface as a function of the inhibitor concentration must be obtained.

The most widespread isotherm, the “Langmuir isotherm” is generally considered to represent the adsorption phenomena in the aqueous phase involved in corrosion or inhibition processes. Its use assumes that the solid surface contains a determined number of adsorption sites and that each site can only accommodate a single adsorbed species. Furthermore, the

adsorbed molecules do not interact with each other and all adsorption sites are thermodynamically equivalent. The adsorption energy is therefore independent of the surface coverage rate θ, which means that the adsorption energy is the same for all sites. Figure 12 illustrates the Langmuir model, known for its relationship between the surface coverage parameter and the inhibitor concentration. This relationship is defined by the formula provided below:

$$\frac{C_{\text{inh}}}{\theta} = \frac{1}{K_{\text{ads}}} + C_{\text{inh}} \tag{5}$$

with θ, $K_{\text{ads}}$ and $C_{\text{inh}}$ being respectively the % coverage of the steel surface by the organic corrosion inhibitors, the adsorption process equilibrium constant and the concentration of the inhibitor (mmol·L$^{-1}$).

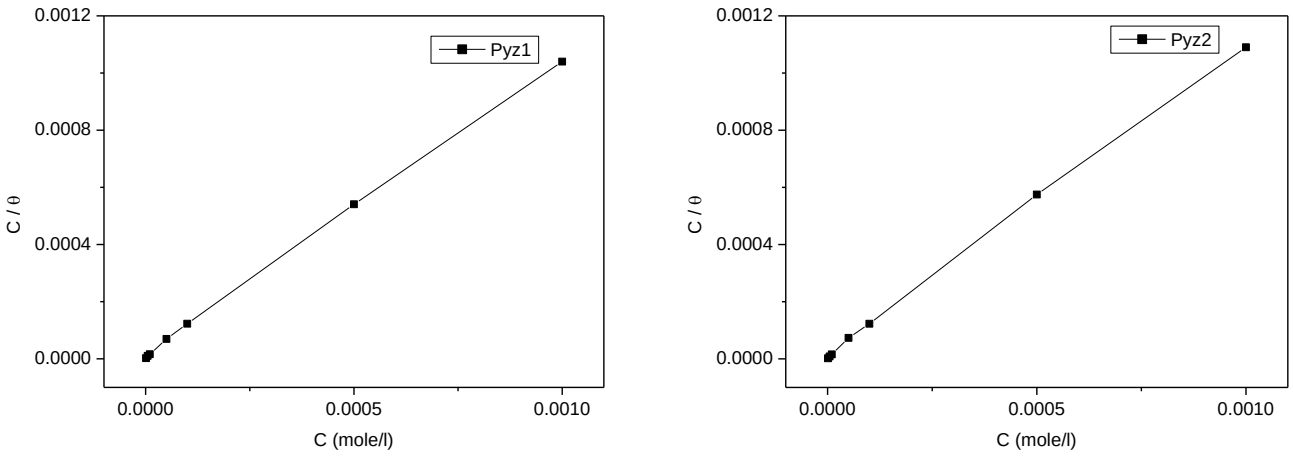


**Figure 12.** Langmuire isotherm of C35E steel in HCl (1 M) in the presence of Pyz1 and Pyz2 at 35°C.

Based on the information presented in Table 4, it is evident that the $K_{\text{ads}}$ values for both compounds are notably high, indicating a significant capacity for these molecules to adsorb onto the steel surface. Conversely, the free energy of adsorption $\Delta G^0_{\text{ads}}$ is linked to $K_{\text{ads}}$ through the subsequent equation:

$$\Delta G^0_{\text{ads}} = -RT \ln(55.5 \times K_{\text{ads}}) \tag{5}$$

where $R = 8.314$ J·K$^{-1}$·mol$^{-1}$, $T = 303$ K, and 55.5 mol/L is the concentration of water in solution.

The analysis of this figure (Figure 12) shows that for the two species the variation of the $C/\theta$ ratio as a function of the inhibitor concentration is linear. This indicates that the adsorption of pyrazolic compounds on the surface of steel in 1 M HCl medium obeys the Langmuir adsorption isotherm. Therefore, the inhibition of corrosion is due to the formation

of a monolayer on the metal surface, limiting the access of the electrolyte. The correlation coefficients ($R^2$) are all close to 1 (>0.999), confirming the validity of the chosen model.

**Table 8.** Adsorption descriptors for the corrosion of steel in presence of both compounds at 308 K.

| Compounds | Slope | $K_{ads}$, $M^{-1}$ | $R^2$ | $\Delta G^0_{ads}$ (kJ/mol) |
|---|---|---|---|---|
| Pyz1 | 1.0191 | $8.22.10^4$ | 0.998 | –39.65 |
| Pyz2 | 1.0876 | $9.65.10^4$ | 0.999 | –39.24 |

### *3.5. Correlation between the molecular structure and anti-corrosion activity*

The aim of this study is to correlate the effect of the structural parameters of pyrazoles by their quantum parameters in order to explain their inhibitory effectiveness. The computer calculation was obtained using the DFT method at the B3LYP level with the (6-31G*(d,p)) base. The calculated quantum chemical parameters, namely the energy of the highest occupied molecular orbital $E_{HOMO}$, the energy of the lowest unoccupied molecular orbital $E_{LUMO}$, the separation energy ($\Delta E = E_{LUMO} - E_{HOMO}$) ,the dipole moment (μ), the softness (σ) and total energy (TE) are summarized in Table 9. The optimized molecular structures with minimum energy of the pyrazoles are given in Figure 13.

**Table 9.** Calculation of quantum indices of pyrazoles.

| Quantum parameters | Pyz1 | Pyz2 |
|---|---|---|
| $E_{HOMO}$, eV | –2.876 | –5.944 |
| $E_{LUMO}$, eV | –1.90 | –1.333 |
| $\Delta E$(gap), eV | 0.976 | 4.611 |
| μ Debye | 5.519 | 3.801 |
| *E*%, W/elec | 98/96 | 89/90 |
| *I*, eV | 2.876 | 5.944 |
| *A*, eV | 1.90 | 1.333 |
| χ, eV | 2.388 | 3.638 |
| η, eV | 0.488 | 2.305 |
| σ, eV | 2.049 | 0.433 |
| $\Delta N$ | 4.725 | 0.7292 |
| TE, eV | 85444.56 | 20165.25 |

In this study, the HOMO energy values may be the most suitable tool to interpret the effectiveness of the pyrazoles obtained. The calculations show that Pyz1 has the highest

HOMO level –2.876 eV (Figure 14), while the lowest HOMO energy corresponds to Pyz2 (–5.944 eV), Figure 15, which has an inhibitory efficiency lower than that obtained by the Pyz1. The lowest LUMO energy value obtained is –1.90 eV (Figure 14). This may explain that the significant inhibition efficiency of the Pyz1 molecule returns to the largest HOMO energy value and the lowest LUMO energy value. The Pyz1 molecule has better inhibitory efficiency with a lower electronegativity value and a larger dipole moment, while Pyz2 has a high electronegativity value and a low dipole moment value. Figure 16 summarizes the diagram of the correlation diagram of the frontier molecular orbitals of the pyrazoles and their energy gap $\Delta E$. These results clearly show that the inhibitory efficiency increases with the decrease in $\Delta E$.

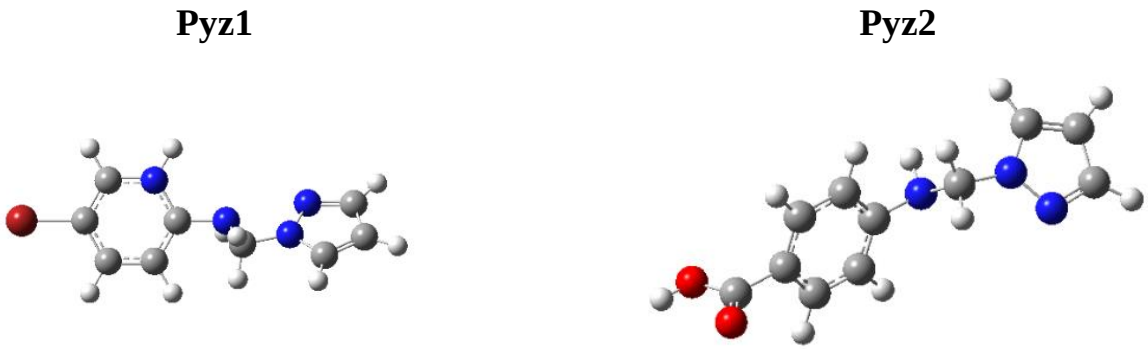


**Figure 13.** Optimized molecular structures of the pyrazoles Pyz1 and Pyz2.

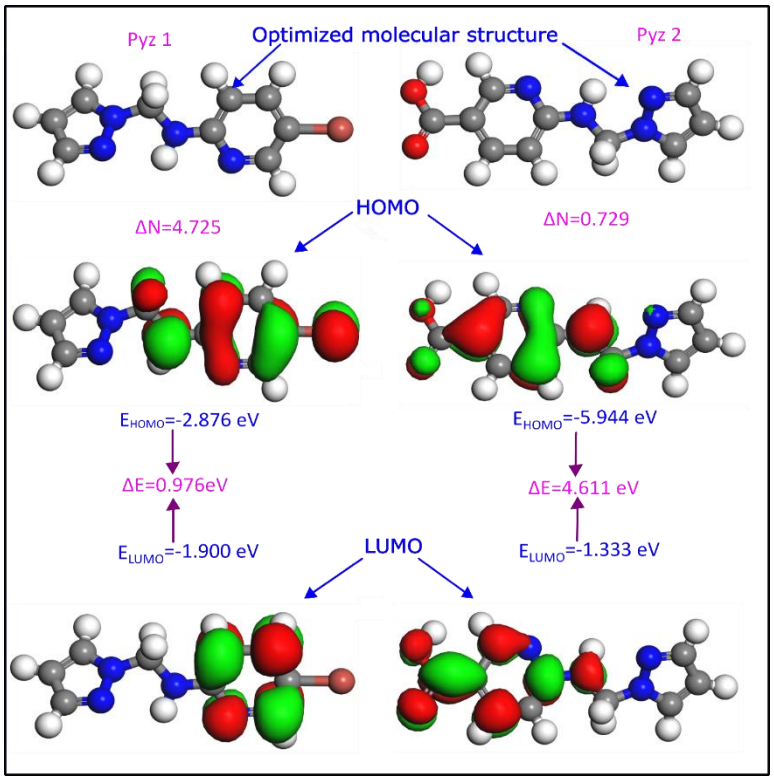


**Figure 14.** HOMO and LUMO density distribution of Pyz1 and Pyz2.

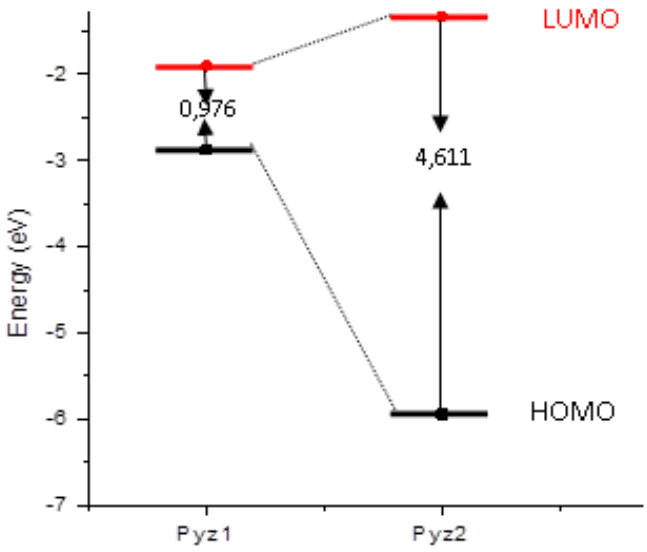


**Figure 15.** Correlation diagram of frontier molecular orbitals of pyrazoles and their energy gap $\Delta E$.

*Local reactivity descriptors*

While HOMO and LUMO are widely used to describe the global reactivity of molecules, local reactivity descriptors provide more detailed information about specific regions within a molecule and their reactivity towards the iron surface. This local reactivity can provide a precise description of the electrophilic or nucleophilic nature of different regions of the inhibitor molecule, allowing us to deduce which specific areas are involved in the adsorption process and how they interact with the iron surface using Hirshfeld analysis. Furthermore, the Fukui functions indices can also be calculated to determine atoms with the highest electrophilicity or nucleophilicity, according to their ($f$+$k$) and ($f$–$k$) values respectively.

Figure 10 displays the local reactivity descriptors represented by bars of different values of Fukui ($f$+$k$) and ($f$–$k$), indicating the electrophilic and nucleophilic regions on the inhibitor molecule. In particular, we found in the Pyz1 molecule that atoms C(1), N(4), C(3), and C(6) show high values of ($f$+$k$) indicating their strong electrophilic character, while atoms Br(15) and N(7) exhibit high ($f$–$k$) values suggesting their nucleophilic nature. Hence, it can be inferred that the mentioned atoms are more likely to interact with the iron surface and participate in the adsorption process. However, in Pyz2 molecule, the the highest electrophilic Fukui functions ($f$+$k$) are observed at atoms O(24), O(25), C(15), and C(1), on the other hand, atoms C(2) and N(7) exhibit highest nucleophilic Fukui functions ($f$–$k$) values among all the atoms in the molecule. This suggests that these specific atoms have a high affinity towards the iron surface and are likely to be involved in the adsorption process.

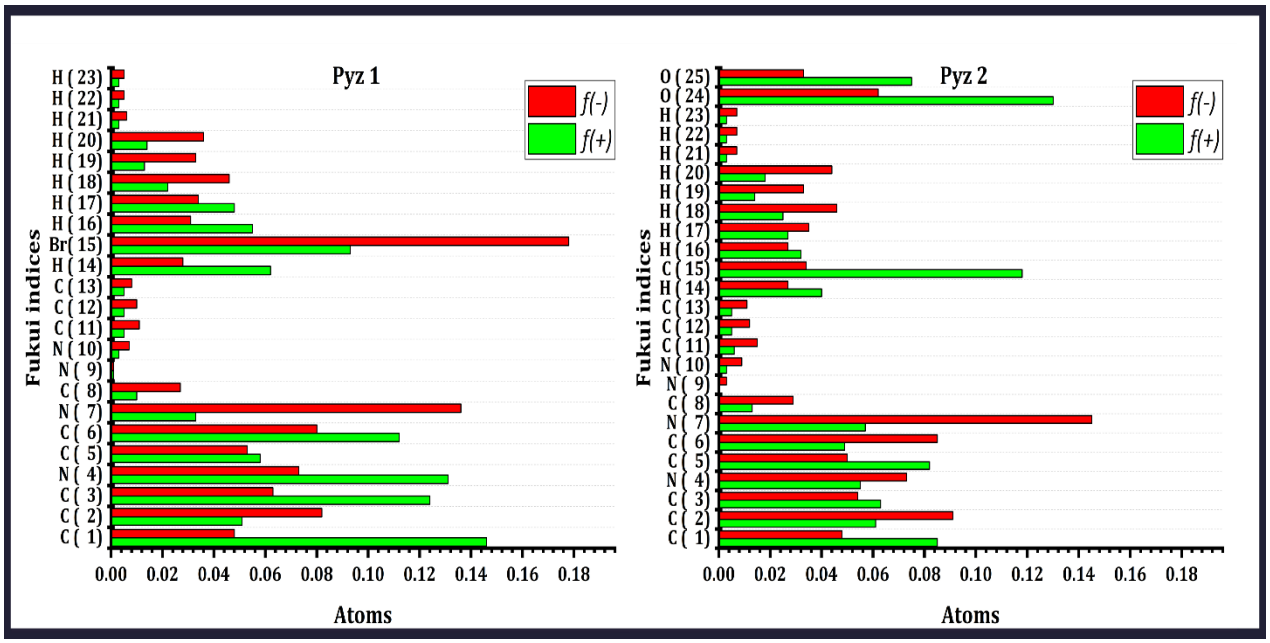


**Figure 16.** Fukui function indices of Pyz1 and Pyz2.

*Molecular dynamics*

To capture the dynamic behavior of the adsorption process, molecular dynamics simulations were performed. Among the strong sides of molecular dynamics simulations is their ability to provide insights into the inhibitor molecule's interactions with the iron surface at a molecular level and to observe how these interactions change over time. This allows us to study the stability of the inhibitor-iron surface complex and understand the diffusion and reorientation behavior of the inhibitor molecules on the surface taking into account the surrounding solvent molecules and thermal energy. Generally, the adsorption of inhibitor molecules on the metallic surface could be through various orientations and conformations, and molecular dynamics simulations help in understanding the preferred orientations and conformations of the inhibitor molecules on the iron surface. In our case, it can be seen in Figure 17 that the Pyz1 and Pyz2 molecules tend to adsorb on the iron surface in a planar orientation parallel to the Fe(110) surface, with the aromatic rings aligning with the iron atoms, which lead to strong π–π interactions between the inhibitor molecules and the iron surface and increase the contact area for adsorption. Therefore, it can be concluded that the Pyz1 and Pyz2 molecules have a high affinity for the iron surface and are likely to form stable inhibitor complexes through Van der Waals forces, electrostatic interactions, and donor-acceptor interactions that are previously discussed in the local reactivity analysis. However, it is important to note that molecular dynamics simulations provide a static representation of the adsorption process and do not account for the dynamic nature of the inhibitor–iron surface interactions in real time. Another limitation of molecular dynamics is its reliance on the accuracy of the force fields used to describe the intermolecular interactions, which can lead to errors in the simulation results. For this reason, we supported

our molecular dynamics simulations with First-principles (*ab initio*) DFT simulations calculations to validate the findings and ensure the accuracy of the results.

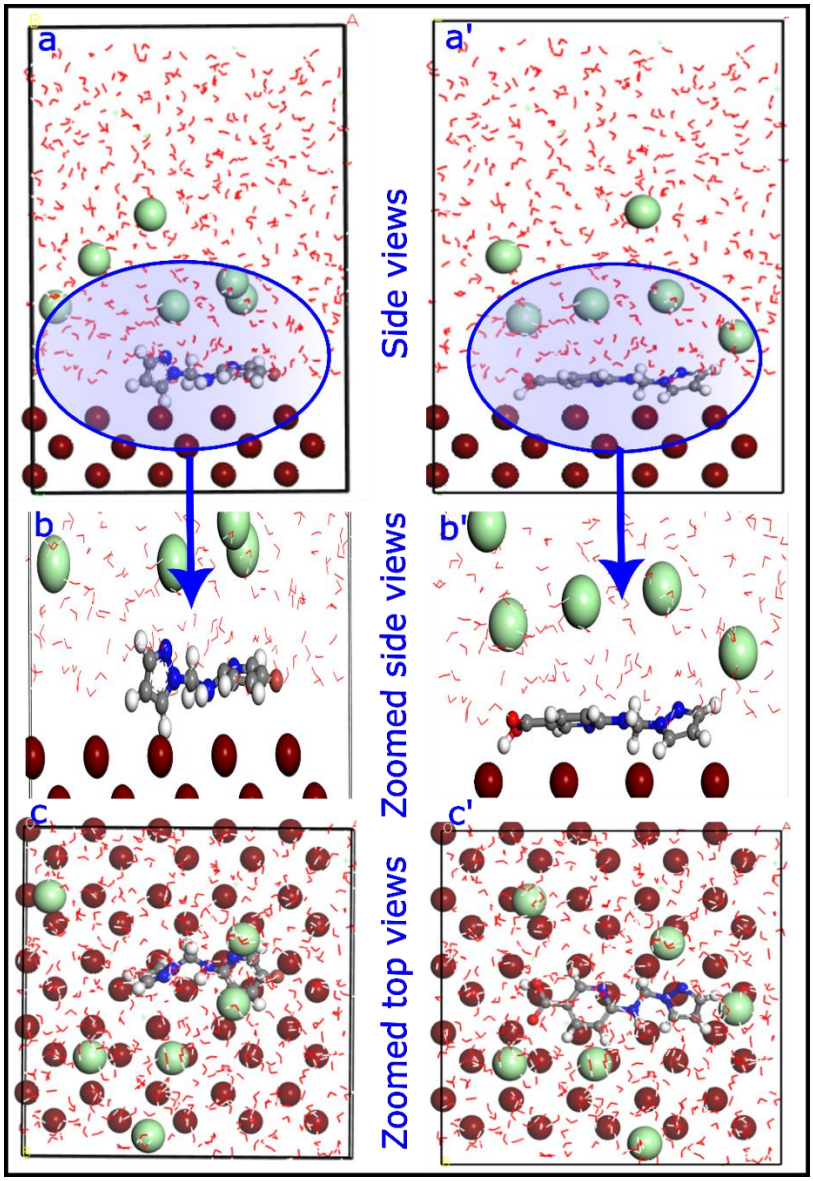


**Figure 17.** Molecular dynamics simulations of Pyz1 and Pyz2.

*First-principles (ab initio) DFT simulations:*

In contrast to molecular dynamics simulations, and quantum calculations, first-principles density functional theory simulations provide a more accurate and detailed description of the inhibitor-iron surface interactions. In addition to the presentation of the most stable adsorption orientations and conformations, the ab initio DFT simulation methods also allow for the calculation of various properties such as adsorption energies or interaction energies, and projected density of state (PDOS), providing a deeper understanding of the inhibitor-metal surface interactions at the atomic level. Figure 17 shows the most stable adsorption

structure of Pyz1 and Pyz2 on the Fe surface obtained from the geometrical optimization using first-principles DFT simulations. It can be noticed that the Pyz1 and Pyz2 molecules are adsorbed on the Fe surface in a planar orientation, similar to what was observed in the molecular dynamics simulations, indicating the stability and consistency of the adsorption behavior. For Pyz1 we observe that the molecule interacts primarily through the oxygen and azote atoms, forming strong covalent bonds with the iron surface, while Pyz2 was adsorbed through several atoms, including oxygen, carbon, and azote, which results in multiple bonds between the inhibitor and the iron surface. The range of formed bonds is 1.351–2.043, 1.920–2.031, and 2.196–2.332 Å for N–Fe, O–Fe, and C–Fe bonds, respectively. On the other hand, the sum of covalent radii for Fe–N, Fe–O, and Fe–C bonds are approximately $r$N+$r$Fe=1.44 Å, $r$O+$r$Fe=1.98 Å, and $r$C+$r$Fe=2.08 Å, respectively. This indicates that the bonds formed between the inhibitor molecules and the iron surface in both Pyz1 and Pyz2 conformations are within a reasonable range, suggesting that they are stable and likely to effectively inhibit corrosion.

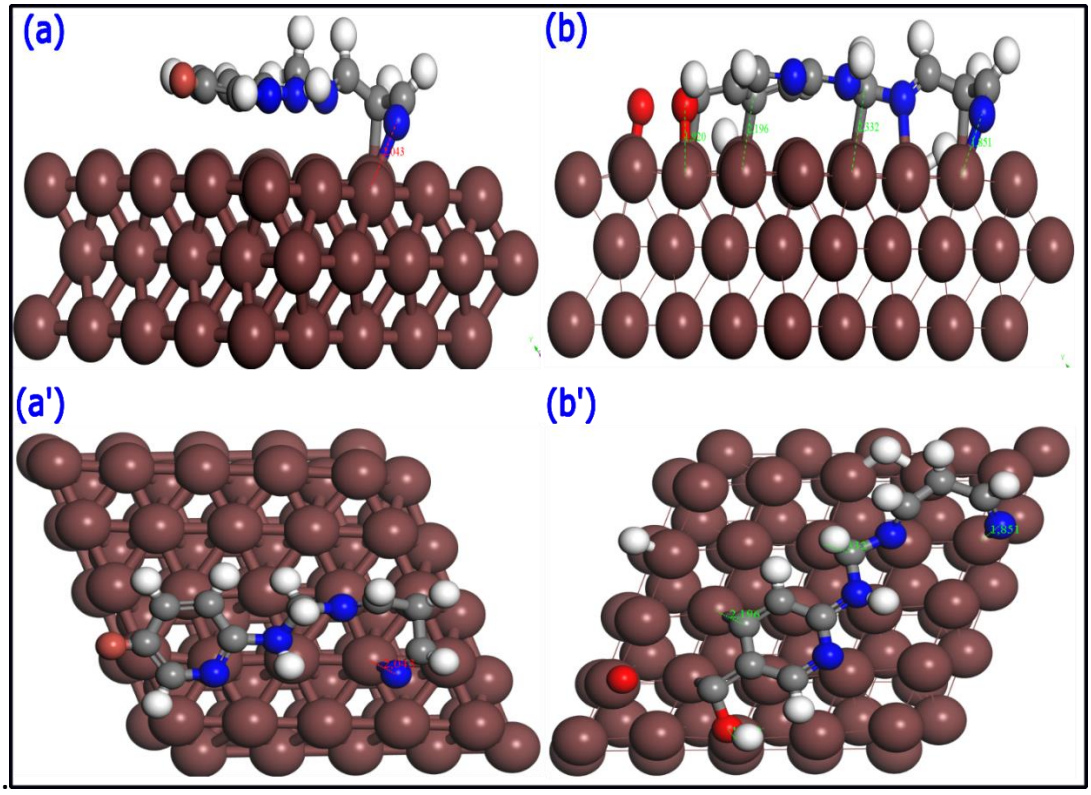


**Figure 18.** DFT-first principal simulations of Pyz1 and Pyz2.

Energetically speaking, the adsorption energies are computed to evaluate the strength of the inhibitor-iron surface interactions. We found that the adsorption energies for both Pyz1 and Pyz2 are negative, indicating exothermic processes and favorable adsorption on the Fe surface, where Pyz1 exhibits a slightly higher adsorption energy (1.02 eV) compared to Pyz2 (1.47 eV). This suggests that Pyz2 has a stronger interaction with the iron surface, making it

a potentially more effective corrosion inhibitor. Additionally, the projected density of state analysis further confirms the strong adsorption behavior of Pyz1 and Pyz2 on the Fe surface, showing significant overlap between the inhibitor's molecular orbitals and the Fe d-orbitals. This indicates a strong electronic interaction between the inhibitor molecules and the iron surface, further supporting their stability and potential effectiveness in inhibiting corrosion. In conclusion, the computational simulations and analysis of the adsorption behavior, bonding distances, adsorption energies, and electronic interactions suggest that both Pyz1 and Pyz2 are effective inhibitors for N80 mild steel in 15 wt.% HCl corrosive media.

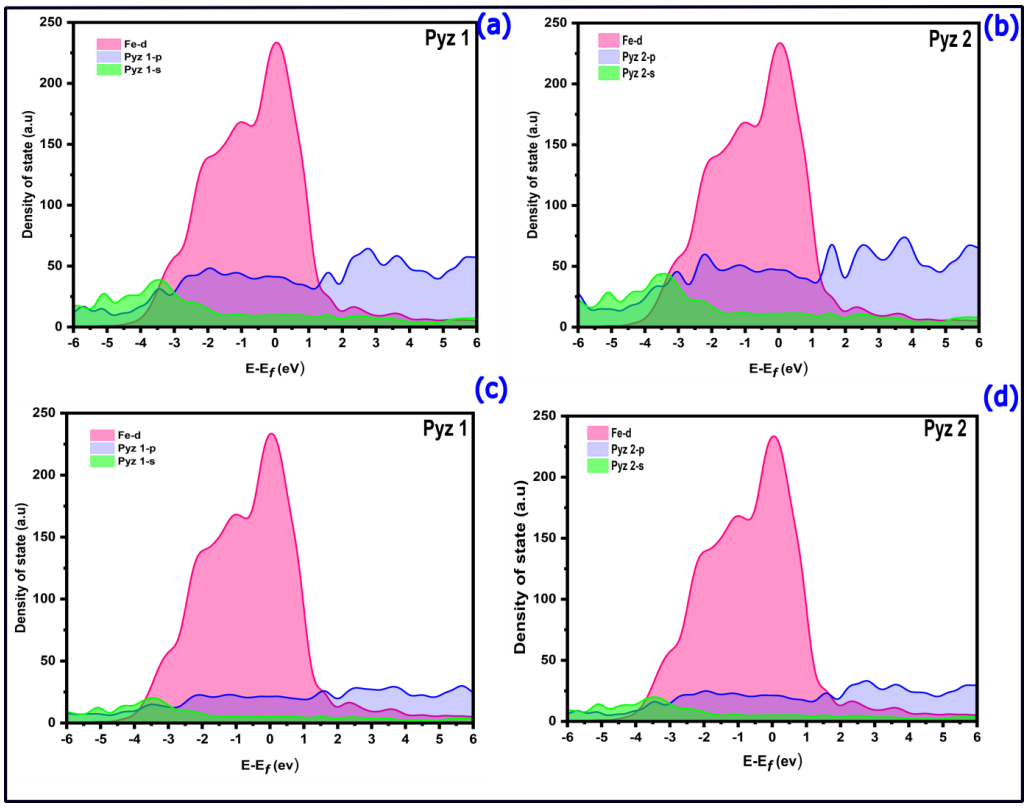


**Figure 19.** DFT-first principal simulations of Pyz1 and Pyz2.

## 4. Conclusion

The physicochemical study of the inhibitory effect of these two pyrazolic compounds was carried out in an acidic medium using different methods. These two heterocycles are excellent inhibitors of steel corrosion in a hydrochloric environment, even at low concentrations. The evaluation of the inhibitory power revealed that Pyz1 is the most effective inhibitor; an inhibitory efficiency of around 98% for the $10^{-3}$ M concentration was obtained. The adsorption of these inhibitors in an acidic medium follows the Langmuir isotherm. The calculated $\Delta G^0_{ads}$ values indicate that these compounds are chemisorbed on the metal surface. Using calculations based on the DFT method, we demonstrated the existence of a correlation between the molecular structure and their inhibitory power.

## References


1. J. Benard, A. Michel, J. Philibert and J. Talbot, Métallurgie générale, *Bulletin de la Société française de Minéralogie et de Cristallographie*, 1970, **93**, no. 3, 409–410.
2. A.A. Nazeer, and M. Madkour, Potential use of smart coatings for corrosion protection of metals and alloys: A review, *J. Mol. Liq*., 2018, **253**, 11–22. doi: 10.1016/j.molliq.2018.01.027
3. V. Saraswat, R. Kumari and M. Yadav, Novel carbon dots as efficient green corrosion inhibitor for mild steel in HCl solution: Electrochemical, gravimetric and XPS studies, *J. Phys. Chem. Solids*, 2022, **160**, 110341. doi: 10.1016/j.jpcs.2021.110341
4. B. Zerga, A. Attayibat, M. Sfaira, M. Taleb, B. Hammouti, M.E. Touhami, S. Radi and Z. Rais, Effect of some tripodal bipyrazolic compounds on C38 steel corrosion in hydrochloric acid solution, *J. Appl. Electrochem*., 2010, **40**, 9, 1575–1582. doi: 10.1007/s10800-010-0164-0
5. N. Benzbiria, A. Thoume, S. Echihi, M.E. Belghiti, A. Elmakssoudi, A. Zarrouk and M. Zertoubi, Coupling of experimental and theoretical studies to apprehend the action of benzodiazepine derivative as a corrosion inhibitor of carbon steel in 1 M HCl, *J. Mol. Struct*., 2023, **1281**, 135139. doi: 10.1016/j.molstruc.2023.135139
6. K. Tebbji, B. Hammouti, H. Oudda, A. Ramdani and M. Benkadour, The inhibitive effect of bipyrazolic derivatives on the corrosion of steel in hydrochloric acid solution, *Appl. Surf. Sci*., 2005, **252**, 1378–1385. doi: 10.1016/j.apsusc.2005.02.097
7. A.A. Al-Amiery, W.N.R.W. Isahak, and W.K. Al-Azzawi, Corrosion Inhibitors: Natural and Synthetic Organic Inhibitors, *Lubricants*, 2023, **11**, 174, doi: 10.3390/lubricants11040174
8. A.S. Jasim, A.A. Khadom, K.H. Rashid and K.F. AL-Azawi, (3,5-dimethyl-1*H*-pyrazol-1-y1) (4-((3,4-dimethoxybenzylidene) amino) phenyl) methanone as a novel corrosion inhibitor for low-carbon steel in hydrochloric acid: Synthesis, diagnosis, and application, *Results Chem*., 2022, **4**, 100569. doi: doi: 10.1016/j.rechem.2022.100569
9. M. Lebrini, F. Robert, A. Lecante and C. Roos, Corrosion inhibition of C38 steel in 1 M hydrochloric acid medium by alkaloids extract from Oxandra asbeckii plant, *Corros. Sci*., 2011, **53**, no. 2, 687–695. doi: 10.1016/j.corsci.2010.10.006
10. A.I. Altsybeeva, E.A. Tronova and V.V. Burlov, Hydrocarbon-soluble metal corrosion inhibitors. II. Physicochemical aspects of inhibitor action. Amides and salts of carboxylic acids, *Int. J. Corros. Scale Inhib*., 2014, **3**, no. 3, 160–166, doi: 10.17675/2305-6894-2014-3-3-160-166
11. P.C. Okafor, E.E. Ebenso, A.Y. El-Etre and M.A. Quraishi, Green Approaches to Corrosion Mitigation, *Int. J. Corros*., 2012, **2012**, 1–2. doi: 10.1155/2012/908290
12. A. Toghan, O.K. Alduaij, A. Fawzy, A.M. Mostafa, A.M. Eldesoky and A.A. Farag, Effect of Adsorption and Interactions of New Triazole-Thione-Schiff Bases on the Corrosion Rate of Carbon Steel in 1 M HCl Solution: Theoretical and Experimental Evaluation, *ACS Omega*, 2024, **9**, no. 6, 6761–6772. doi: 10.1021/acsomega.3c08127

13. A.I. Obike, P.C. Okafor, K.J. Uwakwe, X. Jiang and D. Qu, The inhibition of $CO_2$ corrosion of L360 mild steel in 3.5% NaCl solution by imidazoline derivatives, *Int. J. Corros. Scale Inhib*., 2018, **7**, no. 3, 318–330. doi: 10.17675/2305-6894-2018-7-3-3
14. S. El Issami, L. Bazzi, M. Mihit, B. Hammouti, S. Kertit, E.A. Addi and R. Salghi, Triazolic compounds as corrosion inhibitors for copper in hydrochloric acid, *Pigm. Resin Technol*., 2007, **36**, no. 3, 161–168. doi: 10.1108/03699420710749027
15. H. Namdar-Asl, F. Fakheri, S. Pour-Ali, R. Tavangar and S. Hejazi, Synthesis and Corrosion Inhibition Study of 1-Aminobenzotriazole for Mild Steel in HCl Solution: Electrochemical, Surface Analysis, and Theoretical Investigations, *Prog. Color, Color. Coat*., 2024, **17**, no. 1, 61–74, 2024. doi: 10.30509/pccc.2023.167145.1224
16. V.A. Ogorodnikova, Yu.I. Kuznetsov, A.A. Chirkunov and A.M. Semiletov, Inhibition of anodic dissolution of Mg90 alloy by adsorption layers of higher carboxylic acids, *Int. J. Corros. Scale Inhib*., 2018, **7**, no. 2, 260–270. doi: 10.17675/2305-6894-2018-7-2-11
17. M. Abouchane, N. Dkhireche, M. Rbaa, F. Benhiba, M. Ouakki, M. Galai, B. Lakhrissi, A. Zarrouk and M. Touhami, Insight into the corrosion inhibition performance of two quinoline-3-carboxylate derivatives as highly efficient inhibitors for mild steel in acidic medium: Experimental and theoretical evaluations, *J.Mol. Liq*., 2022, **360**, 119470. doi: 10.1016/j.molliq.2022.119470
18. B. Lin, X. Zhou, T. Duan, C. Zhao, J. Zhu and Y. Xu, Experimental and theoretical study on corrosion inhibition and adsorption performance of *Ipomoea batatas L.* leaf extract for mild steel, *Arabian J. Chem*., 2024, **17**, no. 1, 105410. doi: 10.1016/j.arabjc.2023.105410
19. I. Nadi, M. Bouanis, F. Benhib, K. Nohair, A. Nyassi, A. Zarrouk, C. Jama and F. Bentiss, Insights into the inhibition mechanism of 2,5-bis(4-pyridyl)-1,3,4-oxadiazole for carbon steel corrosion in hydrochloric acid pickling via experimental and computational approaches, *J. Mol. Liq*., 2021, **342**, 116958. doi: 10.1016/j.molliq.2021.116958
20. D. Sharma, A. Thakur, M.K. Sharma, R. Sharma, S. Kumar, A. Sihmar, H. Dahiya, G. Jhaa, A. Kumar, A.K. Sharma and H. Om, Effective corrosion inhibition of mild steel using novel 1,3,4-oxadiazole-pyridine hybrids: Synthesis, electrochemical, morphological, and computational insights, *Environ. Res*., 2023, **234**, 116555. doi: 10.1016/j.envres.2023.116555
21. C. Verma, S.H. Alrefaee, K.Y. Rhee, M.A. Quraishi and E.E. Ebenso, Thiol (-SH) substituent as functional motif for effective corrosion protection: A review on current advancements and future directions, *J. Mol. Liq*., 2021, **324**, 115111. doi: 10.1016/j.molliq.2020.115111
22. H. Jafari, E. Ameri, M.H. Vakili and A. Berisha, Effect of OH position on adsorption behavior of Schiff-base derivatives in corrosion inhibition of carbon steel in 1 M HCl, *Electrochem. Commun*., 2024, **159**, no. 1, 107653. doi: 10.1016/j.elecom.2023.107653

23. H. Ferkous, A. Sedik, A. Delimi, R. Redjemia, K. Abdelsalem, C. Boulechfar, A. Amdjed, A. Malika, A. Boublia, M.S. Ali, B.-H. Jeon, K.K. Yadov and Y. Benguerba, A comparative study of novel synthesized sulfamide compounds: Electrochemical, morphological, XPS, and theoretical investigations on copper corrosion inhibition in 1.0 M HCl, *J. Mol. Liq*., 2023, **394**, 123781. doi: 10.1016/j.molliq.2023.123781
24. T.A. Salman, K.F. Al-Azawi, I.M. Mohammed, S.B. Al-Baghdadi, A.A. Al-Amiery, T.S. Gaaz and A.A.H. Kadhum, Experimental studies on inhibition of mild steel corrosion by novel synthesized inhibitor complemented with quantum chemical calculations, *Results Phys*., 2018, **10**, 291–296. doi: 10.1016/j.rinp.2018.06.019
25. T.A. Salman, A.A. Al-Amiery, L.M. Shaker, A.A.H. Kadhum and M.S. Takriff, A study on the inhibition of mild steel corrosion in hydrochloric acid environment by 4-methyl-2-(pyridin-3-yl)thiazole-5-carbohydrazide, *Int. J. Corros. Scale Inhib*., 2019, **8**, no. 4, 1035–1059. doi: 10.17675/2305-6894-2019-8-4-14
26. A.E.-A. Fouda, A. Al-Sarawy and E. El-Katori, Thiazole Derivatives As Corrosion Inhibitors for C-Steel in Sulphuric Acid Solution. *Eur. J. Chem*., 2010, **1**, no. 4, 312–318. doi: 10.5155/eurjchem.1.4.312-318.105
27. R. Touir, N. Dkhireche, M.E. Touhami, M. Sfaira, O. Senhaji, J.J. Robin, B. Boutevin and M. Cherkaoui, Study of phosphonate addition and hydrodynamic conditions on ordinary steel corrosion inhibition in simulated cooling water, *Mater. Chem. Phys*., 2010, **122**, no. 1, 1–9. doi: 10.1016/j.matchemphys.2010.02.063
28. M.A. Deyab, M.M. Abdeen, M. Hussien, I.E. El-Sayed, A. Galhoum, O.A.A. El-Shamy and M. Abd Elfattah, Novel Corrosion Inhibitor for Carbon Steel in Acidic Solutions Based on α-Aminophosphonate (Chemical, Electrochemical, and Quantum Studies), *Molecules*, 2023, **28**, no. 13, 4962. doi: 10.3390/molecules28134962
29. M. Yadav, D. Sharma, S. Kumar, S. Kumar, I. Bahadur and E.E. Ebenso, Electrochemical and Theoretical Studies on Amino Phosphonates as Efficient Corrosion Inhibitor for N80 Steel in Hydrochloric Acid Solution, *Int. J. Electrochem. Sci*., 2014, **9**, no. 11, 6580–6593. doi: 10.1016/S1452-3981(23)10912-6
30. C. Verma, A. Singh, G. Pallikonda, M. Chakravarty, M.A. Quraishi, I. Bahadur and E. Ebenso, Aryl sulfonamidomethylphosphonates as new class of green corrosion inhibitors for mild steel in 1 M HCl: electrochemical, surface and quantum chemical investigation *J. Mol. Liq*., 2015, **209**, 306–319. doi: 10.1016/j.molliq.2015.06.013
31. A. Dandia, S.L. Gupta, P. Singh and M.A. Quraishi, Ultrasound-Assisted Synthesis of Pyrazolo[3,4-b]pyridines as Potential Corrosion Inhibitors for Mild Steel in 1.0 M HCl, *ACS Sustainable Chem. Eng*., 2013, **1**, no. 10, 1303–1310. doi: 10.1021/sc400155u
32. Y. Abboud, A. Abourriche, T. Saffaj, T. Ainane, M. Charrouf, A. Bennamara, O. Tanane and B. Hammouti, Corrosion inhibition of carbon steel in acidic media by *Bifurcaria bifurcata* extract, *Chem. Eng. Comm*., 2009, **196**, no. 7, 788–800. doi: 10.1080/00986440802589875

33. A.A. Khadom, Kinetics and synergistic effect of iodide ion and naphthylamine for the inhibition of corrosion reaction of mild steel in hydrochloric acid, *eact. Kinet., Mech. Catal*., 2015, **115**, no. 2, 463–481. doi: 10.1007/s11144-015-0873-9
34. A. Fouda, F. El-Taweel and M. Elgamil, Corrosion Inhibition of Aluminum in Hydrochloric Acid Solution Using Some Pyrazolocarbothioamide Derivatives, *Int. J. Electrochem. Sci*., 2017, **12**, no. 12, 11397–11418. doi: 10.20964/2017.12.55
35. M. Mihit, R. Salghi, S. El Issami, L. Bazzi, B. Hammouti, A.A. Addi and S. Kertit, A study of tetrazoles derivatives as corrosion inhibitors of copper in nitric acid, *Pigm. Resin Technol*., 2006, **35**, no. 3, 151–157. doi: 10.1108/03699420610665184
36. N. Timoudan *et al*., Investigation of the mechanisms and adsorption of a new pyrazole derivative against corrosion of carbon steel in hydrochloric acid solution: Experimental methods and theoretical calculations, *Colloids Surf., A*, 2024, **682**, 132771.
37. L. Adlani, N. Benzbiria, T. Abderrahim, N. Timoudan, F. Benhiba, I. Warad, G. Kaichouh, R. Touzani, H. Zarrok, B. Dikici, H. Oudda and A. Zarrouk, Performance of a new pyrazole derivative in 1 M HCl on the corrosion of carbon steel: experimental, quantum chemical and molecular dynamics simulation studies, *J. Dispersion Sci. Technol*., 2024, 1–14. doi: 10.1080/01932691.2024.2304641
38. F. Boudjellal, H.B. Ouici, A. Guendouzi, O. Benali and A. Sehmi, Experimental and theoretical approach to the corrosion inhibition of mild steel in acid medium by a newly synthesized pyrazole carbothioamide heterocycle, *J. Mol. Struct*., 2020, **1199**, 127051. doi: 10.1016/j.molstruc.2019.127051
39. X. Li, S. Deng and H. Fu, Triazolyl blue tetrazolium bromide as a novel corrosion inhibitor for steel in HCl and $H_2SO_4$ solutions, *Corros. Sci*., 2011, **53**, no. 1, 302–309. doi: 10.1016/j.corsci.2010.09.036
40. P.K. Paul, M. Yadav and I.B. Obot, Investigation on corrosion protection behavior and adsorption of carbohydrazide-pyrazole compounds on mild steel in 15% HCl solution: Electrochemical and computational approach, *J. Mol. Liq*., 2020, **314**, 113513. doi: 10.1016/j.molliq.2020.113513
41. F. Abrigach, M. Khoutoul, N. Benchat, S. Radi, N. Draoui, O. Riant and R. Touzani, Library of Synthetic Compounds Based on Pyrazole Unit: Design and Screening Against Breast and Colorectal Cancer, *Lett. Drug Des. Discovery*, 2014, **11**, no. 8, 1010–1016. doi: 10.2174/15701808116666140512220842
42. F. Bentiss, M. Outirite, M. Traisnel, H. Vezin, M. Lagrenée, B. Hammouti, S.S. Al-Deyab and C. Jama, Improvement of Corrosion Resistance of Carbon Steel in Hydrochloric Acid Medium by 3,6-bis (3-Pyridyl)Pyridazine, *Int. J. Electrochem. Sci*., 2012, **7**, no. 2, 1699–1723. doi: 10.1016/S1452-3981(23)13446-8
43. F. Bentiss, M. Bouaniss, B. Mernari, M. Traisnel and M.Lagrenee, *J. Applied Electrochem*., 2002, **32**, 671–678. doi: 10.1023/A:1020161332235

44. K.E. Heusler and G.H. Cartledge, The Influence of Iodide Ions and Carbon Monoxide on the Anodic Dissolution of Active Iron, *J. Electrochem. Soc*., 1961, **108**, 732. doi: 10.1149/1.2428207
45. M. Bartos and N. Hackerman, A Study of Inhibition Action of Propargyl Alcohol during Anodic Dissolution of Iron in Hydrochloric Acid, *J. Electrochem. Soc*., 1992, **139**, 3428. doi: 10.1149/1.2069095
46. P. Vashishth, H. Bairagi, R. Narang, S.K. Shukla, L.O. Olasunkanmi, E.E. Ebenso and B. Mangla, Experimental investigation of sustainable Corrosion Inhibitor Albumin on low-carbon steel in 1N HCl and 1N $H_2SO_4$, *Results Surf. Interfaces*, 2023, **13**, 2023, 100155. doi: 10.1016/j.rsurfi.2023.100155
47. G. Fekkar, F. Yousfi, H. Elmsellem, M. Aiboudi, M. Ramdani, I. Abdel-Rahman and B. Hammouti, L. Bouyazza, Eco-friendly Chamaerops humilis L. fruit extract corrosion inhibitor for mild steel in 1 M HCl, *Int. J. Corros. Scale Inhib*., 2020, **9**, no. 2, 446–459. doi: 10.17675/2305-6894-2020-9-2-4
48. A. Chami, R. Benabbou, M. Taleb, Z. Rais and M. El Haji, Inhibition of corrosion of steel in 1 M HCl solution by polyphenol extract: Application for Steel used in the automotive industry in Morocco, *Mor. J. Chem*., 2023, **11**, no. 3, 623–644. doi: 10.48317/IMIST.PRSM/morjchem-v11i3.37787
49. J. Aljourani, K. Raeissi, M.A. Golozar, Benzimidazole and its derivatives as corrosion inhibitors for mild steel in 1 M HCl solution, *Corros. Sci*., 2009, **51**, no. 8, 1836–1843. doi: 10.1016/j.corsci.2009.05.011
50. K. Tebbji, I. Bouabdellah, A. Aouniti, B. Hammouti, H. Oudda, M. Benkaddour and A. Ramdani, *N*-benzyl-*N*,*N*-bis[(3,5-dimethyl-1*H*-pyrazol-1-yl)methyl]amine as corrosion inhibitor of steel in 1 M HCl, *Mater. Lett*., 2007, **61**, no. 3, 799–804. doi: 10.1016/j.matlet.2006.05.063
51. L. Cui, Y. Lv, Y. Dong, H. Liao, S. Wu and X. Li, Benzothiazole-based ionic liquids as environment-friendly and high-efficiency corrosion inhibitors for mild steel in HCl: Experimental and theoretical studies, *J. Mol. Liq*., 2024, **394**, 123769. doi: 10.1016/j.molliq.2023.123769
52. H.H. Hassan, Inhibition of mild steel corrosion in hydrochloric acid solution by triazole derivatives: Part II: Time and temperature effects and thermodynamic treatments, *Electrochim. Acta*, 2007, **53**, no. 4, 1722. doi: 10.1016/j.electacta.2007.08.021
53. E. Bayol, K. Kayakirilmaz, M. Erbil, The inhibitive effect of hexamethylenetetramine on the acid corrosion of steel, *Mater. Chem. Phys*., 2007, **104**, 74–82. doi: 10.1016/j.matchemphys.2007.02.073

♦ ♦ ♦